Energy, Environmental, and Catalysis Applications

High Capacity Garnet-Based All-Solid-State Lithium Batteries: Fabrication and 3D-Microstructure Resolved Modeling

Martin Finsterbusch, Timo Danner, Chih-Long Tsai, Sven Uhlenbruck, Arnulf Latz, and Olivier Guillon

ACS Appl. Mater. Interfaces, **Just Accepted Manuscript** • DOI: 10.1021/acsami.8b06705 • Publication Date (Web): 11 Jun 2018

High Capacity Garnet-Based All-Solid-State Lithium Batteries: Fabrication and 3D-Microstructure Resolved Modeling

Martin Finsterbusch[a,b], *Timo Danner*[c,d], *Chih-Long Tsai*[a], *Sven Uhlenbruck*[a,b], *Arnulf Latz*[c,d,e], *and Olivier Guillon*[a,b,f]

a. Forschungszentrum Juelich GmbH, Wilhelm-Johnen Str., 52425 Juelich, Germany.

b. Helmholtz Institute Muenster, Wilhelm-Johnen Str., 52425 Juelich, Germany.

c. German Aerospace Centre (DLR), Pfaffenwaldring, 70569 Stuttgart, Germany.

d. Helmholtz-Institute Ulm, Helmholtz-Str., 89081 Ulm, Germany.

e. Institute of Electrochemistry, University of Ulm, Albert-Einstein-Allee, 89069 Ulm, Germany.

f. Jülich-Aachen Research Alliance: JARA-Energy, 52425 Juelich, Germany.

* corresponding authors

Keywords: all-solid-state, ceramic, Li battery, microstructure, modeling, continuum

ABSTRACT

The development of high-capacity, high-performance all-solid-state batteries requires the specific design and optimization of its components, especially on the positive electrode side. For the first time, we were able to produce a completely inorganic mixed positive electrode consisting only of $LiCoO_2$ and Ta-substituted $Li_7La_3Zr_2O_{12}$ (LLZ:Ta) without the use of additional sintering aids or conducting additives which has a high theoretical capacity density of 1 mAh/cm². A true all-solid-state cell composed of a Li metal negative electrode, a LLZ:Ta garnet electrolyte and a 25 µm thick LLZ:Ta + $LiCoO_2$ mixed positive electrode was manufactured and characterized. The cell shows 81% utilization of theoretical capacity upon discharging at elevated temperatures and rather high discharge rates of 0.1 mA (0.1 C). However, even though the room temperature performance is also among the highest reported so far for similar cells, it still falls far short of the theoretical values. Therefore, a 3D reconstruction of the manufactured mixed positive electrode was used for the first time as input for microstructure-resolved continuum simulations. The simulations are able to reproduce the electrochemical behavior at elevated temperature favorably, however, fail completely to predict the performance loss at room temperature. Extensive parameter studies were performed to identify the limiting processes and as a result, interface phenomena occuring at the cathode active material/solid-electrolyte interface were found to be the most probable cause for the low performance at room temperature. Furthermore, the simulations are used for a sound estimation of the optimization potential that can be realized with this type of cell which provides important guidelines for future oxide based all-solid-state battery research and fabrication.

INTRODUCTION

All-solid-state lithium batteries (ASBs) attract increasing attention as a future energy storage technology which is able to overcome several shortcomings of conventional lithium batteries at once. They promise advantages in stability (calendaric and cycle life) and safety (no organic or volatile compounds), while offering a boost in energy density due to a much broader electrochemical stability window enabling the use of high voltage positive electrodes.[1] Within the different possible classes of ceramic solid electrolyte materials,[2-3] the initial skepticism concerning their low ionic conductivity was largely dispelled in the past few years by numerous discoveries of materials with conductivities approaching that of liquid electrolytes. Promising systems include the thio-phosphates based materials, which show the highest total Li ion conductivity (around 10 mS cm^{-1}),[4-9] and the garnet type oxide $Li_7La_3Zr_2O_{12}$ (LLZ) and its substituted derivatives with conductivities around 1 mS cm^{-1}, showing the highest electrochemical stability against various positive and negative electrode active materials.[10-12] In spite of the achieved progress, the potential of all-solid-state batteries is still not fully utilized; in fact, the challenges faced by the ASB development go far beyond the ionic conductivity.[1] One of the serious issues is the compatibility of the electrolyte with Li metal negative electrodes.[13] The only ceramic electrolyte truly stable against Li-metal so far was found to be LLZ,[14] even though some issues can arise at high current density charging if the Li-metal/electrolyte contact is poor.[15-17] Another challenge is the realization of high storage capacities at reasonable charge and discharge rates. This necessitates the use of thick positive electrode layers[18] with interpenetrating phases of conductive and active material exhibiting a large interface and resulting in a high extractable capacity. In conventional Li-ion cells such interpenetrating structures are formed

spontaneously via infiltration of the porous electrodes with liquid electrolyte, which however cannot be adapted in case of fully ceramic electrodes. Formation of the necessary 3D-network in solid cathodes thus requires a careful design of the microstructure and imposes special requirements on the suitable manufacturing procedures. Challenges in fabrication of such mixed cathodes are mainly based on the chemical stability of the present phases during the processing, complicated by a generally significant difference in temperature range of the thermodynamic stability of the different electrode components. Sulfide based solid electrolytes, for example, are known to decompose even at room temperature in contact with certain active materials, forming highly resistive phases[19] or space charge layers[20-21] at the interface. Garnet type LLZ materials on the other hand, are mostly stable at room temperature, but need to be processed at high temperatures during cell manufacturing.[22-24] The enhanced cation mobility during the high temperature sintering step of a mixed cathode containing LLZ can lead to secondary phase formation at the LLZ - active material interface (leading to high interface resistances) or even complete decomposition of the active material itself.[25] Thus, only very few publications are available investigating full cells using LLZ as electrolyte and the mixed cathodes are either still employing liquid electrolytes,[26] organic binders[16] or other solid–Li ion conductors with a lower sintering/melting temperature[27-28] to improve cell performance. Still, theoretical capacity densities for completely inorganic cells are typically low (<< 1 mAh/cm²) and the performance at room temperature is far from these theoretical values. Due to the challenges in fabrication, no sound predictions of the optimization potential of garnet based ASBs are available so far and no clear strategy is available how to achieve relevant energy densities. To circumvent these problems, simulation studies with continuum models based on the physico-chemical parameters of the materials could give valuable insight into the bottlenecks for high cell performance and

thus directions for cell manufacturing and optimization. Most of the continuum models for ASBs presented in the literature focus on thin-film batteries where the transport within the solid electrolyte is typically described by Poisson-Nernst-Planck (PNP)[29] or modified Poisson-Nernst-Planck (mPNP) equations.[30-31] This approach allows for a spatial resolution of the space charge layer at the electrode / electrolyte interface and is advantageous for a detailed study of interfacial effects.[21] However, the computational cost of this approach does not allow to simulate bulk composite electrodes needed for high capacity cells. On this length scale it is therefore common to assume electro-neutrality.[32-34] Composite electrodes are conceptually similar to the electrodes in conventional Li-Ion batteries. The most popular and widely used continuum models typically describe the insertion and transport of Li in the framework of porous electrode theory[35-38]. Instead of resolving the micro-structure of the electrode the simulated volume is homogenized and structural effects on transport processes (e.g. tortuosity) and the rate of insertion/deinsertion reactions are described by correlations based on structural properties like porosity and volume specific surface area. More recently, micro-structure resolved simulation approaches[38-41]were developed which intrinsically take into account structural effects on electrochemical performance. This methodology provides direct access to the influence of e.g. electrode loading and thickness or the active material to electrolyte ratio. Moreover, a transfer of this approach is able to give answers to topics which a specific to and highly relevant for ASBs like the importance of solid electrolyte conductivity in the composite electrode or the influence of structural inhomogeneities e.g. non-impregnated pore space on Li and potential distribution and, thus, battery performance.

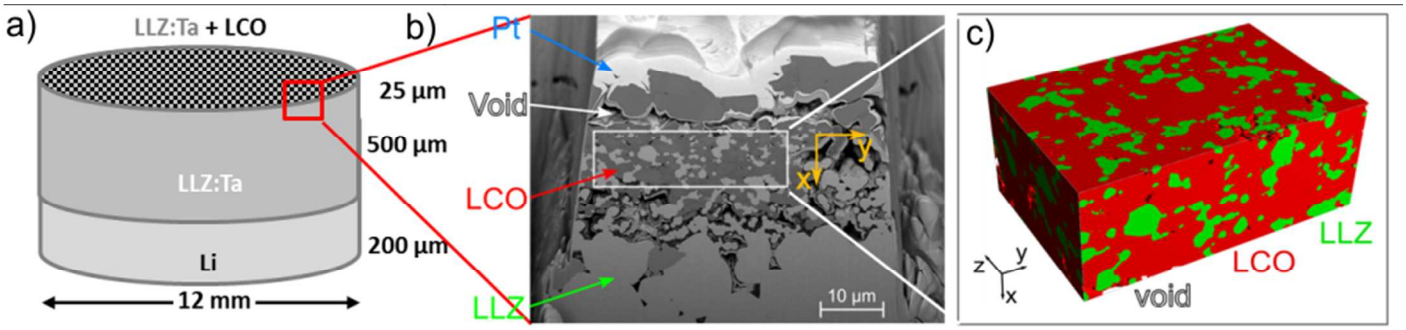

Figure 1 a: Schematic of the manufactured ASB including the respective layer thicknesses. b: SEM micrograph of the FIB-crosscut of the mixed cathode with the area used for electrode reconstruction (white rectangle) and its respective coordinate system (z direction perpendicular into the micrograph plane). c: 3D Reconstruction of the mixed cathode with the LCO and LLZ phase shown in red and green color, respectively.

We present in this study the first successful attempt in preparing a fully inorganic, garnet based all-solid-state battery featuring only a Li metal anode, a Ta-substituted LLZ (LLZ:Ta) electrolyte and a 25 µm mixed cathode of LLZ:Ta+ $LiCoO_2$ (LCO) (schematic shown in Figure 1 a) without any additional phases and a high LCO loading of ~ 7mg cm^{-2}. We then analyze its electrochemical performance on a fundamental level using for the first time a highly developed three dimensional microstructure resolved continuum model on a reconstructed volume of the mixed cathode (shown in Figure 1 b and c). We validate our model based on the experimental results at elevated temperature without any modification or fitting of the input parameters. This validation enables us to perform a systematic study to qualitatively investigate the impact of various parameters such as temperature, conductivity (electronic and ionic), porosity and geometry on the cell performance. Finally, the assessment of parameter sensitivity reveals bottlenecks for battery performance and allows us to derive an optimal strategy for specific improvements of materials, processing routes and cell design in addition to a sound estimation of

achievable performance under optimized conditions. This combined experimental and simulation approach can be easily applied to other all-solid-state systems as well and could dramatically reduce the necessary time for cell optimization – transitioning from a trial and error approach to a strategic one based on mechanistic understanding.

EXPERIMENTAL SECTION

The fully inorganic all-solid-state cells were fabricated using LLZ:Ta ($Li_{6.6}La_3Zr_{1.6}Ta_{0.4}O_{12}$) prepared via a solid-state reaction described in our previous work[15, 22] combining a LLZ:Ta electrolyte support with a mixed cathode of the same LLZ:Ta and $LiCoO_2$ (LCO) (battery grade, MTI Corporation, Richmond USA) and an anode made from Li metal foil (Alfa Aesar, 99.9%). For fabrication of the LLZ:Ta support, 7 g of calcined LLZ:Ta powder was uniaxially pressed in a die with 13 mm diameter under 150 MPa. Sintering was performed at 1150 °C for 5 hours in a closed alumina crucible with a MgO plate in between the LLZ:Ta pellet and the crucible. After sintering, the obtained pellet was sliced into ~0.5 mm thick discs using a diamond saw and polished using up to 4000 grit sandpaper in order to obtain the supporting electrolyte.

Prior to the mixed cathode fabrication, the chemical compatibility of the electrode materials was investigated on a mortared mixture of LLZ:Ta and LCO powders (taken in 1:1 volume ratio) by differential scanning calorimetry (DSC) and thermal gravimetric analysis (TGA) using a heating and cooling rate of 10 K min^{-1} and a 30 minutes dwell time at 1200 °C using a Jupiter STA 449 F1 differential scanning calorimeter (Netzsch). Further compatibility studies using XRD can be found in the respective section of the supplemental material and a more general discussion in one of our previous publications.[42]

Based on the obtained results, an optimized procedure for fabricating the mixed cathodes was developed as follows. The LLZ:Ta and LCO powders were mixed with a volume ratio of LCO/LLZ:Ta = 2 in a polyethylene plastic bottle by using yttria-stabilized zirconia milling balls and ethanol on a bench roller for 24 hours. After drying, alpha terpineol and ethyl cellulose were blended with the mixed powder on a three roll mill to form a paste. The paste was then coated onto the prepared LLZ:Ta pellets using a paintbrush and, after drying, the cells were sintered at 1050 °C in air for 30 minutes to burn out the organics, densify the coating and provide good bonding between the mixed cathode and electrolyte support. An actual mass loading of 7.1 mg cm^{-2} LCO was determined for the mixed cathode. These sintered half-cells were polished in a glove box with up 4000 grit sandpaper on the anode side of the LLZ:Ta electrolyte support to remove possible impurities due to the high temperature heat treatment. The metallic Li foil was then pressed onto the pellets by hand. An Au layer was sputtered on the cathode side to serve as current collector. Then, the cell was sandwiched in between two Ni current collectors and installed in a Swagelok cell. For comparison, a second type of cell was manufactured using the exact same procedures as above, but with a pure LCO cathode slurry, yielding a cell with the same cathode thickness but without the LLZ:Ta ion conductive phase.

The electrochemical performance of the cells was investigated via galvanostatic charge-discharge by applying a current density of 0.1 mA cm^{-2} (0.1 C) at room temperature and at 100 °C (using a BioLogic VMP-300 multi-potentiostat in combination with a climate chamber by Vötsch Industrietechnik VT 4002EMC). In order to correlate the microstructure and the electrochemical performance via 3D modeling, Focused Ion-Beam/ Scanning Electron Microscopy (FIB-SEM) tomography was performed on the cathode of the prepared all-solid-state cell, schematically shown in Figure 1a. The full cell was mounted on an aluminum SEM

sample holder with the mixed cathode side up and an approx. 1 µm thick platinum layer was sputtered on top to assure a good electrical conductivity and reduce charging of the sample. For the subsequent FIB preparation, a dual-beam-FIB Helios 600i from FEI was used to extract a pillar with the total dimensions of (x,y,z) 50x42x30 µm³ as shown in Figure 1 b. The x direction is hereby perpendicular to the surface of the sample and represents the direction of the current flow during cycling of the cell. The front side of the pillar (x-y plane) was then milled in steps of 50 nm (z direction) using a 2.5 nA Ga beam and backscattered electron (BSE) images were taken after each step. A total of 378 images were taken and due to the strong atomic Z-contrast of the BSE image, a clear separation of the LCO active material (medium grey), the LLZ:Ta solid ion conductor (white) and voids (pores, black) was possible using gray scale analysis which is also indicated in Figure 1. The white rectangle in Figure 1 b represents the region of the electrode which was used for 3D reconstruction and chosen to be as homogeneous and dense as possible, representing the desired microstructure. The respective staple of SEM image sections was then imported and reconstructed using the software GeoDict[43] to obtain a full 3D geometry consisting of cubic voxels with an edge length of 50.0 nm and a total volume of 10.9x31.4x16.4 µm³. (The resulting image of the reconstruction is shown in Figure 1 c).

SIMULATION SECTION

In order to estimate the values of an optimized mixed cathode, 3D micro-structure resolved simulations within our simulation framework **B**attery and **E**lectrochemistry **S**imulation **T**ool (BEST)[38-39] were performed. BEST was originally developed at the Fraunhofer ITWM Kaiserslautern for the 3D microstructure resolved simulation of Li-ion batteries.[44] In a joined effort between DLR/HIU and Fraunhofer BEST is now extended to describe additional processes

as well as new battery concepts and chemistries. The governing equations are given by the conservation equations for mass and charge in the active particles and electrolyte. This set of equations is able to describe the dynamic evolution of the concentration and potential distributions in the battery. The equations are derived based on the fundamental principles of non-equilibrium thermodynamics[38-39.] The model was adjusted in order to describe the Li-ion transport in the solid electrolyte within our framework. Most importantly, the solid electrolyte was assumed to be a single ion conductor and the lithium transference number was thus set to $t_{\mathrm{Li}^+} = 1$. This assumption is backed up by the electronic conductivity of LLZ which was found to be more than 6 orders of magnitude smaller than the lithium ion conductivity.[45] A detailed description is given in the supplementary material.

To simulate the experimental setup, a virtual representation of the full cell consisting of the 3D reconstruction of the composite cathode, separator, and Li metal anode was implemented in our simulation framework BEST. The main focus of the simulations was set on the quantification of transport processes in the real microstructure of the mixed cathode, obtained via 3D FIB-SEM reconstruction and anode and separator were modeled as isotropic layers. Note, that by doing the simulations directly on the microstructure of the composite cathode the tortuosity of the electrode is intrinsically taken into account. . In order to obtain reliable bulk transport parameters of the LLZ:Ta solid electrolyte independent measurements were performed. The total Li-ion conductivity of LLZ:Ta at 25°C, 50°C and 100°C was measured to be $\kappa_{25}^{\mathrm{elyte}} = 5.4 \cdot 10^{-2}$ S m^{-1}, $\kappa_{50}^{\mathrm{elyte}} = 1.8 \cdot 10^{-1}$S m^{-1} and $\kappa_{100}^{\mathrm{elyte}} = 1.1$ S m^{-1} respectively, using the same LLZ:Ta pellets as in the full cells but with Au blocking electrodes setup.[15] The Li-ion diffusion coefficient was calculated from these measured lithium ion conductivities based on the assumption of negligible interactions between lithium ions and lattice vacancies using $D_{\mathrm{Li}}^{\mathrm{elyte}} = \kappa^{\mathrm{elyte}} RT / c_{\mathrm{Li}}^{\mathrm{elyte},0} F^2$ with

T the absolute temperature, *F* the Faraday constant and *R* the gas constant. The lithium ion concentration in the electrolyte $c_{\mathrm{Li}}^{\mathrm{elyte},0} = 38.4$ kmol m^{-3} was estimated from the density [46] and composition of LLZ. Finally, the transport and electrochemical parameters of LCO were taken from the literature. Molenda *et al.* report an electric conductivity of Li_xCoO_2 as function of temperature and lithium concentration *x*.[47] In their study they found only a very modest temperature dependence of the electric conductivity up to x=0.97. In our simulations we use a constant conductivity $\sigma_{\mathrm{LCO}}^{\mathrm{elode}} \approx 100\ \mathrm{S/m}$ (x=0.8) at all concentrations and temperatures. Van der Ven et al. calculated a concentration dependent chemical diffusion coefficient of Li in LCO at 400 K, however, the authors estimate that the uncertainty in their values is one to two orders of magnitude. Therefore, we use in our simulations a constant value of $1 \cdot 10^{-10}$ cm^2/s. [38] All other parameters related to the electrochemistry of LCO were taken from the modeling literature of Li-ion batteries with conventional liquid electrolytes[37]. Since reliable data on the properties of LCO at high temperatures (50 and 100°C) is scarce we use the literature values at room temperature as a conservative approximation although e.g. an increase in the Li diffusion coefficient with temperature can be expected. Intensive parameter studies are reported in the supplementary material investigating the influence of individual parameters on cell performance. A summary of parameters and sources is given in Table 1.

Table 1 - Input parameters of the simulations.

Parameter	Description	Value
Electrolyte		
$\boldsymbol{c_{\mathrm{Li}}^{\mathrm{elyte},0}}$ / mol m^{-3}	Concentration of Li sites in LLZ*	38400
$\boldsymbol{\kappa^{\mathrm{elyte},0}}$ / S m^{-1}	Li-ion conductivity**	100°C: **1.1** / 50°C: 0.18 / 25°C: 0.054

$\boldsymbol{t_{Li}} / -$	Transference number**	1
$\boldsymbol{D_{Li}^{elyte}}$ / m^2 s^{-1}	Li-ion diffusion coefficient*	100°C: $\mathbf{7.90 \cdot 10^{-12}}$/ 50°C: $\mathbf{1.24 \cdot 10^{-12}}$/ 25°C: $\mathbf{3.80 \cdot 10^{-13}}$
(1 + ($\boldsymbol{\partial}$ln $\boldsymbol{f_{Li}^{elyte}}$ /$\boldsymbol{\partial}$ln $\boldsymbol{c_{Li}^{elyte}}$)) / -	Activity term*	1
$\boldsymbol{L_{LLZ}}$ / m	Electrolyte thickness**	$\mathbf{500 \cdot 10^{-6}}$
LCO		
$\boldsymbol{c_{Li}^{elode,0}}$/ mol m^{-3}	Initial Li concentration in LCO*	27058
$\boldsymbol{\sigma_{LCO}^{elode}}$ / S m^{-1}	Electronic conductivity [47]	100
$\boldsymbol{D_{Li}^{elode}}$ / m^2 s^{-1}	Li-ion diffusion coefficient[37]	$\mathbf{1 \cdot 10^{-14}}$
$\boldsymbol{i_{00}^{LCO}}$ / A m$^{2.5}$ mol$^{-1.5}$	Exchange current density factor [37]	$\mathbf{9.81 \cdot 10^{-7}}$
$\boldsymbol{U_0^{LCO}}$ / V	Open circuit potential [37]	Eq. (A.2) in Ref.[31]
$\boldsymbol{\alpha^{LCO}}$ / -	Symmetry factor [37]	0.5
$\boldsymbol{c_{Li}^{elode.max}}$ / mol m^{-3}	Maximum Li concentration[37]	51555
$\boldsymbol{L_{LCO}}$ / m	Composite electrode thickness**	$\mathbf{25 \cdot 10^{-6}}$
Li metal		
$\boldsymbol{\sigma_{Li}^{elode}}$ / S m^{-1}	Electronic conductivity*	$\mathbf{1 \cdot 10^{4}}$
$\boldsymbol{i_{00}^{Li}}$/ A m^{-2}	Exchange current density factor[48]	10
$\boldsymbol{U_0^{Li}}$ / V	Open circuit potential	0.0
$\boldsymbol{\alpha^{Li}}$ / -	Symmetry factor	0.5

Values are taken from the respective Reference (Superscript [# of REF]), measured by the authors (Superscript [**]) or calculated (Superscript [*]). Transport properties of LLZ:Ta are given at 25, 50, and 100°C. All other parameters are constant in the simulations.

Taking into account all assumptions which have been made and the uncertainty in some of the parameters, the results can only be expected to be of qualitative nature, especially since polarization effects (space charge layers) and the formation of degradation products at the

interface, as well as mechanical stress and strain due to volume changes upon lithiation and delithiation are not modeled. A more rigorous approach for ionic transport and interface phenomena in solid electrolytes can be found in a recent publication.[21]

RESULTS AND DISCUSSION

Chemical stability testing

For the preparation of composite cathodes, the knowledge of maximum sintering temperature is essential to provide the highest density films while avoiding a solid state reaction between the LCO and LLZ:Ta. DSC and TGA were performed using the LCO/LLZ:Ta powder mixture as described in the experimental section and is shown in Figure 2. Below 1000 °C, only a very small peak was observed at around 700 °C, which might be due to a (rather sluggish) reaction of the two powders to form $LaCoO^3$.[49] However, in accordance with literature, the reaction is too slow for any additional phase to be detected with XRD on the timescales typically used for our ASB manufacturing and no additional peaks were observable even for 2 hours dwell time at 900, 1000 or 1050 °C (cf. Figure S1 in the supplementary material). A major peak can be found in the DSC curve at 1085 °C and is associated with a steep slope in the weight loss curve, which does not recover during the cooling down of the sample, indicating an irreversible reaction between the two materials. No secondary phases are detected up to 1050 °C, the onset of the DSC peak. Further investigation of the formed phases is not within the scope of this paper but details on the stability of LCO and LLZ:Ta can be found in one of our previous publications.[42] From the DSC/TGA (and supplemental XRD) results the maximum sintering temperature was determined to be 1050 °C, which was then chosen as sintering temperature for the mixed cathode during cell

fabrication. This rather high temperature was needed to ensure good densification of the mixed cathode and a reasonable sintering of the mixed cathode to the LLZ:Ta electrolyte pellet.

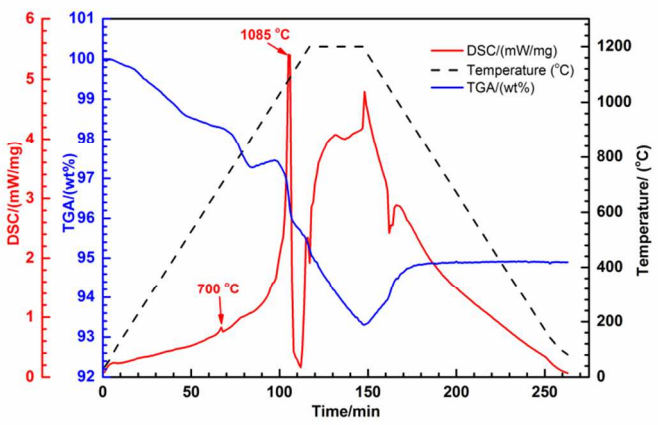

Figure 2 - Differential scanning calorimetry (DSC) and thermal gravimetric analysis (TGA) of a mixture of LLZ:Ta and LCO up to 1200 °C, showing stability of the two materials up to 1085°C.

However, it cannot be excluded from the available data that some secondary phase formation might take place at the LLZ:Ta/LCO interface, forming a thin layer in between the two phases. Unfortunately, investigations of this interface or possible secondary phases within are currently not possible with the available equipment but should be undertaken to elucidate its exact structure and possible impact on the cell performance. Still, it is possible that due to the lower sintering temperature compared to the pure LLZ:Ta pellet some grain boundaries in the LLZ phase remain which will reduce the Li ion conductivity within the mixed cathode. An analysis of this effect via our simulation approach can be found in the supplementary material.

Electrochemical tests

The first charge/discharge curves of the two prepared cell types are shown in Figure 3 a. For the all-solid-state cell made with a 25 µm pure LCO cathode, very poor utilization of the cathode was observed. At 100 °C and a high current density of 0.1 mA cm^{-2}, only 0.05 mAh cm^{-2} capacity density or approx. 3% of the total available capacity was utilized. In contrast, the cell featuring the mixed LCO/LLZ:Ta cathode showed a capacity density of 0.84 mAh cm^{-2}, corresponding to approx. 81% utilization of the available cathode capacity when normalized to the actual mass loading of 7.1 mg cm^{-2} LCO determined experimentally during cell manufacturing. This is, to our knowledge, by far the highest loading and best performance for a garnet based fully inorganic mixed cathode.

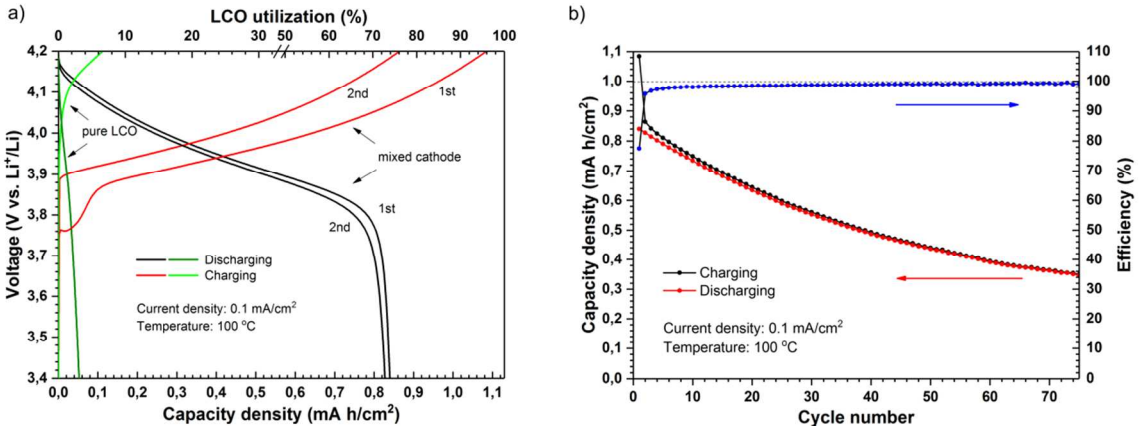

Figure 3 a) Dis-/charge curves of first cycle of a cell with pure LCO cathode and the first and second cycle of a cell with mixed cathode, b) capacity vs. cycle number plot for 75 cycles of the cell with mixed cathode.

For definition of the utilization axis, to have a fair comparison to the dense, pure LCO cathode, the effect of porosity was excluded by calculating the mass loading of a 25 µm thick and 100% dense mixed cathode (8.3 mg cm^{-2} corresponding to 1.13 mAh cm^{-2} capacity density) and this value set as 100% in Figure 3 a. The fact that the electrochemical performance of a cell with a

mixed cathode is superior compared to pure LCO is not surprising, since it is known that the diffusion coefficient for Li^+ in LCO is rather low.[37] However, processing of cathode active materials and oxide ceramic solid state electrolytes like LLZ:Ta is still challenging due to their reactivity at high temperature. It is thus of vital importance to link the microstructural properties of the mixed cathode to the electrochemical behavior of the cell in order to assess the impact of modifications and enable targeted cell development. The significance of understanding this linkage can be seen in the cycling performance data of the cell, shown in Figure 3 b. The cell shows a rather fast degradation, loosing approx. half its capacity within the first 50 full cycles (100% DOD). Since the coulombic efficiency stays at >99% and the cell has a large Li supply at the anode, the degradation is most likely not due to parasitic side reactions and/or Li loss, but due to mechanical failure of the materials due to the swelling and contraction of the active material. A similar behavior was observed for sulfide based all-solid-state cells featuring mixed cathodes, where a capacity fade despite very high coulombic efficiencies was observed.[50-52] Since thin film cathode based cells show a very stable cycling behavior,[53] this mechano-chemical degradation seems to be typical issue for ASBs with mixed electrodes. However, no obvious signs of failure were visible in the SEM and a detailed study to elucidate the failure mechanism is needed.

Mixed cathode microstructure and 3D reconstruction

The image of the reconstructed composite electrode is shown in Figure 1 c. LCO active material was found with a volume percentage of 63% and is shown in red color. Green parts represent the solid LLZ electrolyte which accounts for 30 vol-% of the electrode structure. The remaining 7 vol-% of the geometry are empty spaces (pores). Based on the reconstruction data,

the specific interface areas (LCO-LLZ: $1.1 \cdot 10^6$ m^{-1}; LCO-void: $4.9 \cdot 10^5$ m^{-1}; LLZ-void: $3.4 \cdot 10^4 m^{-1}$) and effective transport parameters such as the relative electrolyte conductivity $\kappa^{\mathrm{elyte,eff}}/\kappa^{\mathrm{elyte,0}}$ (LLZ (x/y/z): (0.052/0.051/0.053) and electrode conductivity $\sigma^{\mathrm{elode,eff}}/\sigma^{\mathrm{elode,0}}$ (LCO (x/y/z): (0.45/0.40/0.42) were evaluated using GeoDict. A summary of the results for the reconstructed volume and additional geometry cases discussed below is provided in Table S1 in the supplementary material.

It is important to note that the reconstructed part seen in Figure 1 is more homogeneous compared to other regions of the electrode layer, especially at the electrolyte – mixed cathode interface; therefore, real cell performance is expected to be worse than the modeled one. First, due to the larger overall residual porosity, the theoretical capacity is much smaller (~15%) than what would be expected based on the extrapolation of the reconstructed volume. Second, the connectivity of the active cathode phase might be more limited than expected from the reconstruction (more isolated particles) which also reduces the capacity. Finally, it can also cause a decrease of the effective transport parameters and active surface area, which will result in higher transport and activation overpotentials and will shift the discharge curve to lower voltages. The reconstructed cathode used in the model can thus be seen as a first promising configuration featuring a percolated Li ion-conductive phase and a maximized amount of active material, but some remaining voids (7% porosity). Although the void volume is relatively small, simulating a complete impregnation of the void space with LLZ electrolyte (filled w/ LLZ) would increase the specific surface area by ~45 %. A similar effect can be observed for the relative conductivity of LLZ . The value was found to almost double in the case of increased electrolyte content ($\kappa^{\mathrm{elyte,eff}}/\kappa^{\mathrm{elyte,0}}$ filled w/LLZ (x/y/z): 0.10/0.075/0.09). On the other hand, when filling the void space with pure LCO (filled w/ LCO), the overall capacity increases

significantly (by 0.11 mAh cm^{-2}). Both these cases (labeled as filled w/ LLZ and filled w/ LCO) give valuable insight on the effect of changing the respective volume fractions during cathode preparation and the resulting effect on overall cell performance and will be discussed in the following section.

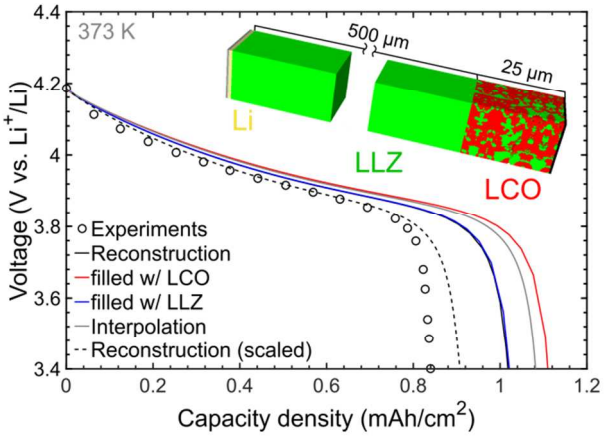

Figure 4 - Full cell model used for the simulation (inset), measured discharge curve for the first cycle at 100°C (open circles) and simulated data for as reconstructed (black) and void-filled mixed cathode (red = LCO, grey= mixed, blue= LLZ).

Full cell simulation

To model the full all-solid-state cell, the reconstructed part of the mixed cathode was mirrored twice at the *y-z* plane and subsequently cropped to get the correct electrode thickness of 25 µm in

through-plane direction *x*. The inset in Figure 4 schematically depicts the geometry of the simulated full cell with the 500 µm thick LLZ:Ta electrolyte and the lithium metal anode (out of scale). The measured discharge curve of the first cycle with a current density of 0.1 mA cm^{-2} (corresponding to approx. C/10 rate) is also shown in Figure 4 (open circles). In order to quantify the influence of the remaining porosity, three sets of simulations were conducted. First, the original electrode reconstruction was used including porosity (black solid line). Second, the void space was filled with LLZ:Ta electrolyte (blue solid line) and third, it was filled with pure LCO (red solid line). The additional active material increases the theoretical capacity by approximately 0.11 mAh cm^{-2}. Since the void space cannot be filled with a 2:1 mixture of LCO:(LLZ:Ta) as the exact distribution is unknown, the performance of a fully dense mixed cathode can only be approximated by the weighted linear combination of the two curves for the artificially filled cases (grey solid line). The simulation using the reconstructed microstructure of the mixed cathode (black solid line) accurately models the shape of the discharge curve while overestimating the capacity of the cell, which is due to the choice of the reconstructed area (as discussed above). The corresponding Li distribution at the end of discharge shows an almost complete lithiation of the LCO. Therefore, it is expected that the capacity of the cell at small currents (0.1 mA cm^{-2}) scales linearly with active material content. The LCO loading in the electrode samples was determined experimentally to ~7.1 mg cm^{-2}. Based on the tomographic data we calculate a mass loading of the simulated electrodes of ~8 mg cm^{-2}, resulting in a ratio in active material loading of 0.887. Scaled results of the as reconstructed electrode (black dashed line) show improved agreement with the experimental discharge curves, strengthening our argument that some of the deviation originates from the difference in active material content. Still, the scaled simulations overpredict capacity by about 6% which could be caused by

unconnected particles close to the cathode/separator interface where the fraction of void space is largest. Filling the void spaces with LLZ:Ta indicates that increasing the LLZ:Ta content (while reducing porosity) shows a very slight increase in performance, owing to improved transport properties and a higher active interface area. However, improvements are minor which demonstrates that the reconstructed region, which was deliberately chosen due to its denser and more homogeneous structure, is almost ideally impregnated with LLZ electrolyte and forms a percolating network for Li-ion conduction. Due to this existing network, filling the void spaces with LCO almost linearly increases the capacity, as around 91% of the additional LCO can be reversibly lithiated and delithiated. Figure 5 shows the corresponding local distributions of Li ion current density in the LLZ electrolyte (a) and Li fraction x in the Li_xCoO_2 cathode (b) for the as reconstructed electrode geometry during discharge at 3.939 V. Bright red areas in the current density distribution of the solid electrolyte (Figure 5 a) represent regions with high absolute values. The percolating network for Li ion conduction is revealed in the microstructure of the mixed cathode. As expected, highest Li ion current densities are found close to the separator with decreasing intensity towards the cathode current collector. The graph also shows several white spots at the electrolyte-active material interface, indicating low current densities due to an

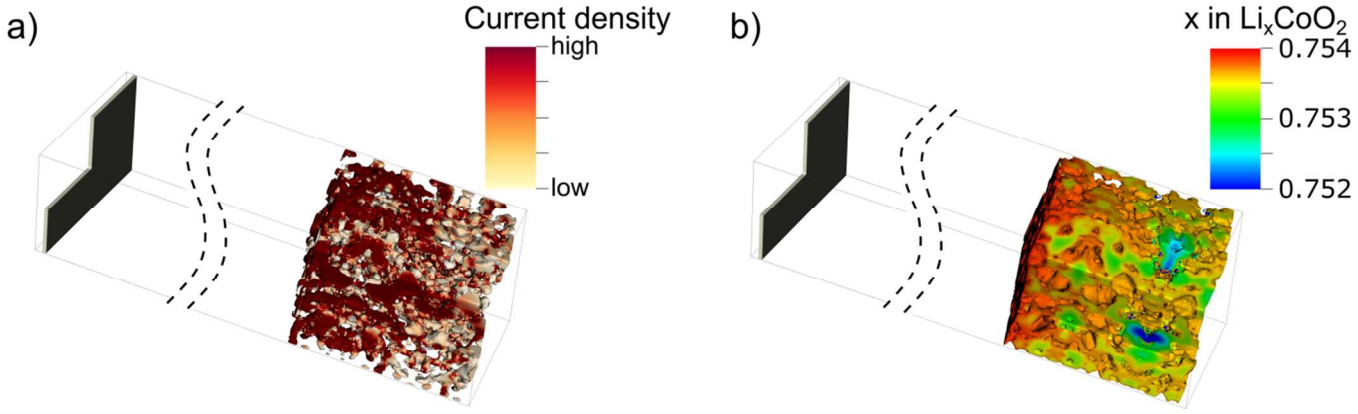

Figure 5 - a: Distribution of local current densities in the LLZ electrolyte phase within the mixed electrode. b: corresponding Li concentration x in the Li_xCoO_2 of the 25 µm mixed cathode at 50% depth-of-discharge with 0.1 mA cm^{-2} (0.1C) at 100°C.

inhomogeneous contact between the two phases. However, this inhomogeneity of the contact area is still less pronounced than for the actual contact area visible in the SEM micrograph (Fig. 1 b) due to the choice of the reconstructed volume. Additional white areas can be seen throughout the mixed cathode and coincide with regions of lower Li concentration (blue areas) within the cathode active material (cf. Figure 5 b). This coincidence is caused by an inhomogeneous LLZ distribution and locally poor contact to the active material, resulting in a locally slower discharge. A similar trend can be observed across the whole cathode, with areas close to the electrolyte having slightly higher, and close to the current collector slightly lower Li ion concentrations. On average, however, the Li concentration is close to x=0.75 which is expected at 50% depth-of discharge and at the end of discharge almost complete lithiation of the active material was observed (x∼1). This finding is in line with the very high utilization of the active material (cf. scaled discharge curve in Figure 4). At a small current of 0.1 mA/cm^2 the homogeneous Li distribution also indicates the beneficial effect of the Li diffusion in the active material, aiding in areas of poor contact between electrolyte and active material. The complex interplay of the different transport mechanisms in the micro- structure of the mixed cathode is clearly demonstrated and highlights the advantages of the 3D modeling approach presented in this work. As the current goal of ASB development is increasing cell capacity, a sound understanding of the effect of volumetric fractions of ion conducting phase and active material is needed for targeted maximization of extractable capacity. The three cases (reconstructed, filled w/ LLZ and filled w/ LCO) will thus be investigated in case of different temperatures, cell geometries and material improvements. First, the working temperature was reduced from 100°C to 25°C. In the simulations this was taken into account by adjusting the transport parameters of LLZ:Ta to the corresponding values at 25°C ($\kappa_{25}^{\mathrm{elyte},0} = 5.4 \cdot 10^{-4}$ S cm^{-1}, $D_{\mathrm{Li}}^{\mathrm{elyte}} = 3.2 \cdot$

10^{-10} m^2 s^{-1}) which are roughly a factor of 20 smaller compared to 100°C ($\kappa_{100}^{\mathrm{elyte},0} = 1.1 \cdot 10^{-2}$ S cm^{-1}, $D_{\mathrm{Li}}^{\mathrm{elyte}} = 8.4 \cdot 10^{-9}$ m^2 s^{-1}). All other parameters were used as provided in Table 1. Representative simulation results of the as reconstructed electrode geometry are shown in Figure 6 a. Simulations of the filled w /LLZ and filled w/ LCO cases showed the same qualitative trends like the simulations at 100°C discussed above.

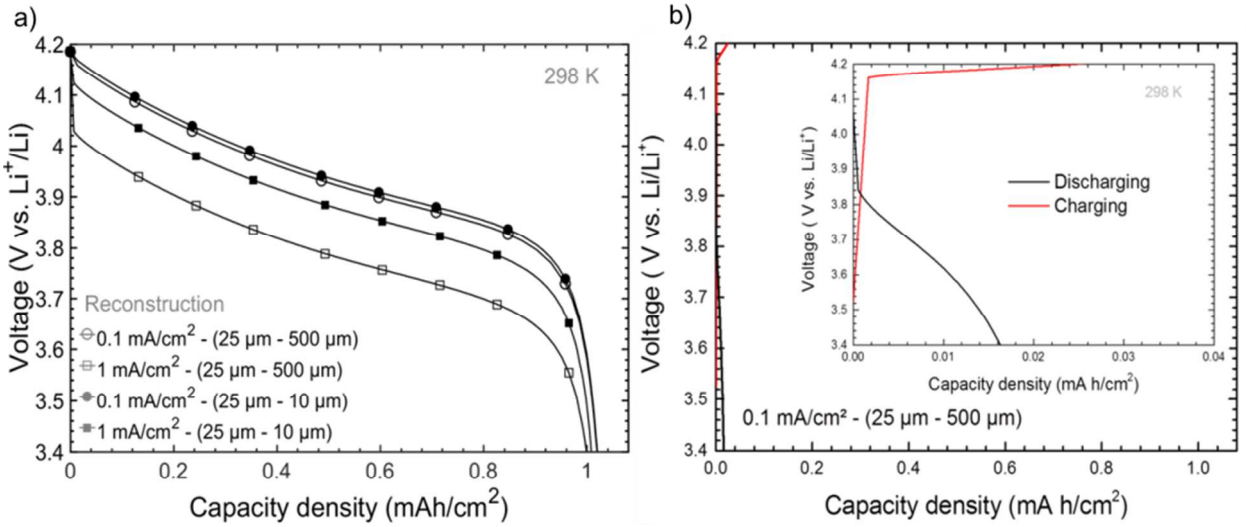

Figure 6 - a: Simulated discharge curves of reconstructed electrodes at room temperature for discharge currents of 0.1 mA cm^{-2} (circles) and 1 mA cm^{-2} (squares). The influence of electrolyte thickness is exemplarily shown for a 500 µm (open symbols) and 10 µm (filled symbols) electrolyte. b: measured dis-/charge curves at room temperature for a cell with the same dimensions but a 1:1 ration of LLZ:Ta to LCO in the mixed cathode.

At 0.1 mA cm^{-2}, also used for the simulations in Figure 4, the simulated performance at room temperature decreases only slightly from the one at 100°C. This decrease is in accordance with the estimated ohmic losses in the LLZ phase (separator + mixed electrode) of only a 9 mV. However, comparison to the measured data for a similar cell at room temperature (Figure 6 b) shows a large deviation from the predicted behaviour. The performance at RT is so poor that, in order to maintain the discharge rate of 0.1 mAh cm^{-2}, the ratio of LLZ:Ta to LCO needed to be

changed to 1:1 in order to obtain results visible on the same x-scale as in Figure 6 a. From the inset in Figure 6 b, we assume that one polarization effect dominates the whole curve. Our theoretical approach allows separating the contribution of different processes to the overall performance of the mixed electrode. In the supplementary material we present a comprehensive and detailed parameter study in order to identify the limiting process of the battery performance at room temperature. It can be concluded from those investigations that the drastic performance loss and differences in characteristics of the RT discharge curve cannot be explained by variation of a single parameter alone. In addition, in our model we assumed an ideal interface between LLZ and LCO and do not include any side reactions, space charge layers, or electromechanical degradation phenomena. Therefore, we conclude, in accordance with the few previous studies,[16, 27-28] that the large loss in performance in fully inorganic cells with a pure LLZ:Ta/LCO cathode is also due to interface processes and the dominating polarization effect is most likely an additional charge transfer resistance with a high activation energy at the interface. Further analysis will be required to clarify this result, but the present results give already important directions for future research, highlighting the importance and need for interface engineering between cathode and electrolyte. To assess the impact of LLZ:Ta transport parameters and mixed electrode geometry for a future well-developed interface, first, the discharge current was increased to 1C (1 mA cm^{-2}). The simulated discharge curve (open squares) showed qualitatively similar features but the predicted capacity at the 3.4 V cut-off voltage is slightly smaller due to an inhomogeneous lithiation of the active material (cf. Figure S8 in the supplementary material).

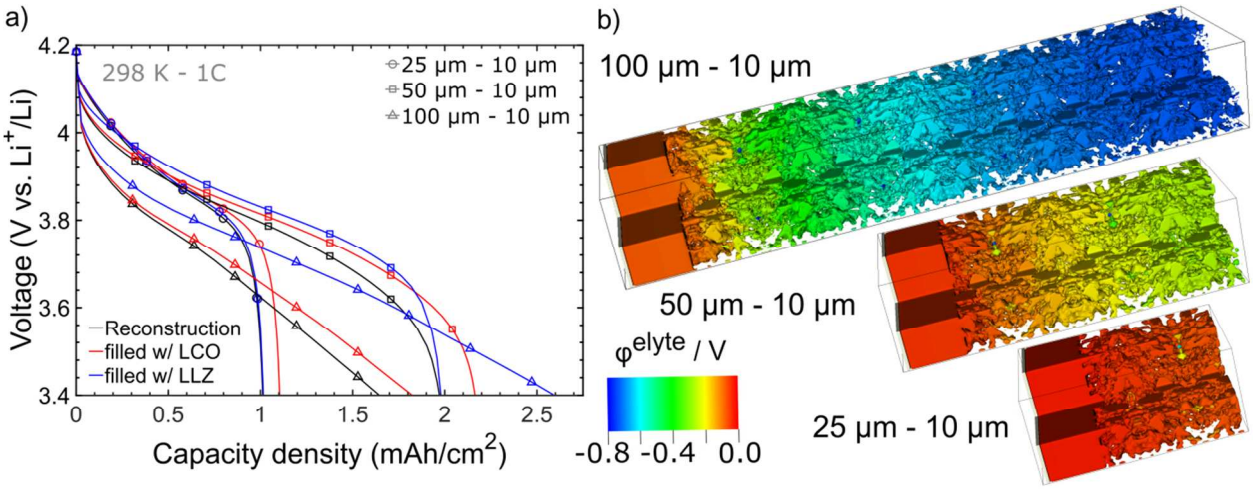

Figure 7 - a: Simulated discharge curves of mixed cathodes with a thickness of 25µm, 50 µm, and 100 µm, respectively. For each thickness simulations were run for the as reconstructed electrode geometry and the design cases filled w/ LLZ and filled w/ LCO. b: Potential distribution in the LLZ electrolyte phase for the as reconstructed electrode geometries at the end of a 1C discharge.

Most importantly, ohmic losses of $\Delta\phi = i \cdot L_{\mathrm{sep}}/\kappa_{25}^{\mathrm{elyte},0}$ ≈0.1 V in the 500 µm thick LLZ:Ta solid electrolyte caused a significant decrease in cell performance for 1 mA cm^{-2}. Therefore, as second step, the electrolyte thickness was reduced in our simulations to a target value of only 10 µm. The corresponding results are represented by solid symbols in Figure 6 a. A small reduction of ohmic losses for 0.1 mA cm^{-2} and a large reduction of almost 75% for 1 mA cm^{-2} can be observed. In all-solid-state battery research, the target of reducing the solid electrolyte thickness to only a few (tens of) µm can thus be seen as second priority after interface engineering, especially when ASBs with high energy density at room temperature are desired. The increase of electrode thickness in order to overcome the capacity limitations of thin-film solid state batteries is another focal point in ASB research. Therefore, in a third simulation step, the electrode thickness was increased in two steps to a final electrode thickness of 100 µm corresponding to a

theoretical capacity of around 4 mAh cm^{-2}, which would be at par with conventional Li-ion batteries.[54] Figure 7 a compares three different cell designs for a 1C discharge at room temperature. The 25 µm electrode with a 10 µm separator showed an almost full utilization of the theoretical capacity and only marginal ohmic losses and serves as reference configuration. Figure 7 b shows the potential distribution in the LLZ:Ta electrolyte at the lower cut-off voltage of a 1C discharge of the as reconstructed electrodes. For the 25 µm reference the potential distribution is rather homogeneous giving a visual confirmation for sufficient Li ion conduction and the formation of a percolating network of LLZ:Ta electrolyte. Therefore, as discussed above, the filled w/ LCO case gives the highest capacity and discharge voltage. Doubling the electrode thickness while maintaining the 10 µm thick electrolyte (50 µm – 10 µm) almost linearly increases the capacity of the battery. The differences between the three geometry cases (as reconstructed, filled w/ LCO, filled w/ LLZ) become more pronounced compared to the 25 µm electrode. Looking at the potential distribution in the LLZ:Ta electrolyte, an increase in the potential gradient can be observed. This indicates that at 1C the 50 µm mixed electrode is at the onset of a transport limitation of Li in the electrolyte phase. The filled w/ LCO case still delivers the highest capacity. However, filling the pores with LLZ improves the Li transport and the predicted cell voltage surpasses the discharge voltage of the filled w/ LCO case. Up to 50 µm electrode thickness the increase in capacity scales almost linearly and an extrapolation would predict approx. 4 mAh cm^{-2} for the 100 µm electrode. However, the simulated capacity of around 1.5 mAh cm^{-2} was found to drop even below the practical capacity of the 50 µm electrode, which is due to the increase in current density by a factor of two (double capacity at same C rate). The potential distribution in the LLZ:Ta electrolyte (cf. Figure 7 b) provides evidence for a transport limitation of Li ions. Significant parts of the mixed cathode close to the current collector are not

accessible for Li ions and thus do not contribute to the overall capacity of the cell. The situation improves only marginal if the void space is filled with LCO (filled w/ LCO) since the network for Li ion transport is essentially the same (cf. Figure S11, supplementary material). In contrast, the simulation of the 'filled w/ LLZ' case showed a capacity increase of 1 mAh cm^{-2} to a total of 2.5 mAh cm^{-2} and generally higher discharge voltages. This indicates that depending on the applied discharge current an optimal electrolyte to active material ratio exists which can be determined with the help of a simulation based approach. The results presented in Figure 7 demonstrate the importance of Li-ion transport in the solid electrolyte phase of the mixed cathode at high currents and electrode loadings. Therefore, we finally investigate in our simulations the effect of improved Li-ion conductivity. The conductivity in our room temperature simulations ($\kappa_{25}^{\mathrm{elyte},0} = 5.4 \cdot 10^{-4}$ S cm^{-1}) was increased to $\kappa_{50}^{\mathrm{elyte},0} = 1.8 \cdot 10^{-3}$ S cm^{-1} and $\kappa_{100}^{\mathrm{elyte},0} = 1.1 \cdot 10^{-2}$ S cm^{-1} corresponding to the conductivities of LLZ:Ta measured at 50°C and 100°C, respectively. This increase by a factor of 3 and 20 in total Li ion conductivity would put them at par with commercial liquid-gel electrolytes (~1x10^{-3} S cm^{-1})[8] and the best sulfide based solid electrolyte (1x10^{-2} S cm^{-1})[8]. Results of the conductivity study are presented in Figure 8. Increasing the ionic conductivity of the solid electrolyte resulted only in minor improvements in the performance of the as prepared cell (25 µm electrode, Figure S13 supplementary material). This trend is similar to the results of the filled w/ LLZ case (cf. Figure 3). However, there was a significant gain in performance in case of the cell with a 100 µm mixed cathode. Increasing the conductivity by a factor of 3 ($\kappa_{50}^{\mathrm{elyte},0} = 1.8 \cdot 10^{-3}$ S cm^{-1}) and 20 ($\kappa_{100}^{\mathrm{elyte},0} = 1.1 \cdot 10^{-2}$ S cm^{-1}) improves the capacity by more than a factor of 2. However, an increase to even higher conductivity values did not provide significant improvements for the cell configurations studied in this work. Figure 8 (b) provides the distribution of Li in the LCO active

material corresponding to the three conductivity cases explained above. The distributions show an improved utilization of the active material at elevated conductivities. For improvements in conductivity by a factor of 3 ($\kappa_{50}^{\mathrm{elyte},0} = 1.8 \cdot 10^{-3}$ S cm^{-1}) the Li distribution at the end of discharge was found to be already almost homogeneous. This demonstrates that the ionic conductivity of the electrolyte in the mixed cathode needs to be improved, once a certain area loading and/or thicknesses is reached, respectively. Moreover, it provides concrete numbers for a targeted electrolyte development for oxide based ASBs while putting the search for highly Li conducting materials in an overall perspective. Thus, to be at par with conventional liquid based Li-ion batteries, we estimate that a total Li-ion conductivity of $\kappa^{\mathrm{elyte}} = 2.0 \cdot 10^{-3}$ S cm^{-1} would be sufficient for ASBs based on oxide ceramic electrolytes.

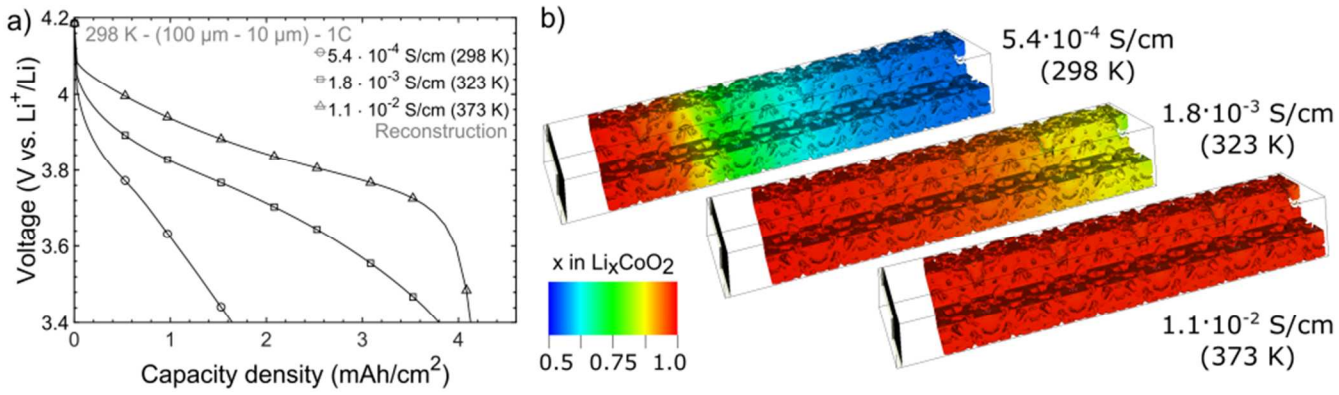

Figure 8 - Influence of LLZ conductivity on the performance of the mixed electrode. a: Delithiation curves. b: Distribution of Li in the active material at the lower cut-off voltage.

CONCLUSIONS

For the first time, a fully inorganic, garnet based all-solid-state battery having a 25 µm thick, mixed cathode of LCO/LLZ:Ta was fabricated and reversibly cycled at 100°C and 25°C with C/10. A capacity density of 0.84 mAh cm^{-2} (81% of its theoretical capacity) was reached at

elevated temperature during the first cycles, which is also the highest reported so far for fully inorganic cells based on oxide ceramics. Even though a better cell performance can be achieved by adding organic electrolytes, the introduction of such additional phases makes the de-convolution of the contributions of each phase on the total cell performance very challenging.

Due to this unique structure of our cells, it was possible for first time to successfully perform 3D microstructure resolved continuum simulations of the electrodes and full cells without any modification or fitting of the input parameters. The electrochemical performance at room and elevated temperature in combination with an extensive parameter study (cf. supplemental material) enabled us to determine the impact and thus importance of possible optimization strategies for this cell type.

First priority is the optimization of the electrolyte – active material interface to minimize the large polarization which is the main cause for the performance loss at room temperature. (Demonstrated by the models ability to reproduce the high temperature experimental data favorably but showing large deviations at room temperature, since the interface is not included in the model yet.) The materials choices for the mixed cathode are currently limited by the chemical stability of the materials during processing, and even small amounts of secondary phases at the interface (not detectable in XRD) or space charge regions can lead to large charge transfer resistances. Unfortunately, a detailed analysis of the interface structure and property determination for inclusion in the model is very challenging, due to the fast degradation of the material under high energy electron or ion bombardment. However, similar to sulfide based ASBs, proper interface engineering is an utmost priority also for oxide based ASB.

Second priority is the improvement of rate performance and energy density of the full cells. Reduction of the electrolyte thickness has by far the largest impact on increasing this critical

indicator, as demonstrated by our optimized model cell with a 10 µm electrolyte. However, as this is a reduction by at least a factor of 25-50 in thickness compared to state of the art cells, research on advanced electrolyte processing methods also needs to be a major topic in future ASB research.

Third priority is to manufacture high energy density oxide-based mixed cathodes. Here the overall porosity needs to be reduced and the bonding to the electrolyte improved. As expected, fully dense mixed cathodes with high active material content will give the highest capacity, as long as percolation of the ion conductive phase is maintained. Almost full percolation was achieved for 25 µm thick mixed cathodes with a LCO to LLZ:Ta volume ratio of 2:1 and can possibly be pushed even further towards higher LCO contents as demonstrated by the filled w/ LCO simulations, leading to even higher energy densities.

Forth priority could be to further increase the energy density by increasing the mixed cathode thickness to obtain high energy cells (>3 mAh/cm²). Since the resulting charge and discharge currents at the same C rates are larger, the volume percentage and conductivity of the ionic conductive phase starts to play a bigger role. Our study showed that now higher LLZ:Ta contents or conductivity is needed for a higher effective Li-ion conductivity in the mixed cathode. With respect to the latter, an enhancement by a factor of 5 (reaching $> 2.0 \cdot 10^{-3}$ S cm^{-1}) would be ideal.

In conclusion, the manufactured cells only based on LLZ:Ta, LCO and Li metal already show promising performances. The joint experimental and modeling approach presented here identified two parameters for cell design and manufacturing which will provide the highest gain for oxide based ASB in the near future: first, improving the interface design to diminish charge transfer resistances and second, reducing the electrolyte thickness to bring down ohmic losses.

Once the cells are optimized with respect to these two parameters, reducing the cathode porosity and increasing the cathode thickness can then improve the energy density further towards relevant values for commercialization. We envision that the applied simulation approach can be expanded and used to predict advanced geometries, e.g. with optimized gradients in active material content, to facilitate lithium ion transport in the composite electrode.

ASSOCIATED CONTENT

Supporting Information. Additional experimental information on the phases and phase distribution in the mixed cathode as well as a detailed derivation of the model equations and a thorough sensitivity study of the simulation towards parameter variations (like active material loading, Li+ diffusion coefficients, electrical conductivity, electrode thickness) (PDF).

AUTHOR INFORMATION

Corresponding Authors

*Martin Finsterbusch, Tel.: +49 2461 61 2877. Fax: +49 2461 61 2455. E-mail: m.finsterbusch@fz-juelich.de

*Timo Danner, Tel.: +49 2461 61 2877. Fax: +49 2461 61 2455. Email: timo.danner@dlr.de

Author Contributions

The manuscript was written through contributions of all authors. All authors have given approval to the final version of the manuscript. * Both corresponding authors contributed equally.

ACKNOWLEDGMENT

The financial support of this work by the Federal Ministry of Education and Research (BMBF), Germany, under grant number 03X4634C and 01DR13013, the Ministry of Innovation, Science and Research of Northrhine-Westfalia under grant number 424-Japan and the Helmholtz Association is hereby gratefully acknowledged. The authors acknowledge support with computational resources provided by the state of Baden-Württemberg through bwHPC (bwForCluster JUSTUS) and the German Research Foundation (DFG) through grant no INST 40/467-1FUGG.

REFERENCES

1. Janek, J.; Zeier, W. G., A Solid Future for Battery Bevelopment. *Nat Energy* **2016,** *1*, 16141.
2. Sendek, A. D.; Yang, Q.; Cubuk, E. D.; Duerloo, K. A. N.; Cui, Y.; Reed, E. J., Holistic Computational Structure Screening of More Than 12 000 Candidates for Solid Lithium-Ion Conductor Materials. *Energy & Environmental Science* **2017,** *10* (1), 306-320.
3. Bachman, J. C.; Muy, S.; Grimaud, A.; Chang, H. H.; Pour, N.; Lux, S. F.; Paschos, O.; Maglia, F.; Lupart, S.; Lamp, P.; Giordano, L.; Shao-Horn, Y., Inorganic Solid-State Electrolytes for Lithium Batteries: Mechanisms and Properties Governing Ion Conduction. *Chemical Reviews* **2016,** *116* (1), 140-162.
4. Murayama, M.; Kanno, R.; Irie, M.; Ito, S.; Hata, T.; Sonoyama, N.; Kawamoto, Y., Synthesis of New Lithium Ionic Conductor Thio-LISICON - Lithium Silicon Sulfides System. *Journal of Solid State Chemistry* **2002,** *168* (1), 140-148.
5. Seino, Y.; Ota, T.; Takada, K.; Hayashi, A.; Tatsumisago, M., A Sulphide Lithium Super Ion Conductor is Superior to Liquid Ion Conductors for Use in Rechargeable Batteries. *Energy & Environmental Science* **2014,** *7* (2), 627-631.
6. Busche, M. R.; Weber, D. A.; Schneider, Y.; Dietrich, C.; Wenzel, S.; Leichtweiss, T.; Schroder, D.; Zhang, W. B.; Weigand, H.; Walter, D.; Sedlmaier, S. J.; Houtarde, D.; Nazar, L. F.; Janek, J., In Situ Monitoring of Fast Li-Ion Conductor Li7P3S11 Crystallization Inside a Hot-Press Setup. *Chemistry of Materials* **2016,** *28* (17), 6152-6165.
7. Kanno, R.; Maruyama, M., Lithium Ionic Conductor Thio-LISICON - The Li2S-GeS2-P2S5 System. *Journal of the Electrochemical Society* **2001,** *148* (7), A742-A746.
8. Kamaya, N.; Homma, K.; Yamakawa, Y.; Hirayama, M.; Kanno, R.; Yonemura, M.; Kamiyama, T.; Kato, Y.; Hama, S.; Kawamoto, K.; Mitsui, A., A Lithium Superionic Conductor. *Nature Materials* **2011,** *10* (9), 682-686.
9. Sahu, G.; Lin, Z.; Li, J.; Liu, Z.; Dudney, N.; Liang, C., Air-Stable, High-Conduction Solid Electrolytes of Arsenic-Substituted Li4SnS4. *Energy & Environmental Science* **2014,** *7* (3), 1053-1058.

10. Miara, L. J.; Richards, W. D.; Wang, Y. E.; Ceder, G., First-Principles Studies on Cation Dopants and Electrolyte Cathode Interphases for Lithium Garnets. *Chemistry of Materials* **2015,** *27* (11), 4040-4047.
11. Han, F. D.; Zhu, Y. Z.; He, X. F.; Mo, Y. F.; Wang, C. S., Electrochemical Stability of Li10GeP2S12 and Li7La3Zr2O12 Solid Electrolytes. *Advanced Energy Materials* **2016,** *6* (8).
12. Tian, Y.; Shi, T.; Richards, W. D.; Li, J.; Kim, J. C.; Bo, S.-H.; Ceder, G., Compatibility Issues Between Electrodes and Electrolytes in Solid-State Batteries. *Energy & Environmental Science* **2017,** *10* (5), 1150-1166.
13. Zhamu, A.; Chen, G. R.; Liu, C. G.; Neff, D.; Fang, Q.; Yu, Z. N.; Xiong, W.; Wang, Y. B.; Wang, X. Q.; Jang, B. Z., Reviving Rechargeable Lithium Metal Batteries: Enabling Next-Generation High-Energy and High-Power Cells. *Energy & Environmental Science* **2012,** *5* (2), 5701-5707.
14. Richards, W. D.; Miara, L. J.; Wang, Y.; Kim, J. C.; Ceder, G., Interface Stability in Solid-State Batteries. *Chemistry of Materials* **2016,** *28* (1), 266-273.
15. Tsai, C. L.; Roddatis, V.; Chandran, C. V.; Ma, Q. L.; Uhlenbruck, S.; Bram, M.; Heitjans, P.; Guillon, O., Li7La3Zr2O12 Interface Modification for Li Dendrite Prevention. *Acs Appl Mater Inter* **2016,** *8* (16), 10617-10626.
16. van den Broek, J.; Afyon, S.; Rupp, J. L. M., Interface-Engineered All-Solid-State Li-Ion Batteries Based on Garnet-Type Fast Li+ Conductors. *Advanced Energy Materials* **2016,** *6* (19).
17. Luo, W.; Gong, Y. H.; Zhu, Y. Z.; Fu, K. K.; Dai, J. Q.; Lacey, S. D.; Wang, C. W.; Liu, B. Y.; Han, X. G.; Mo, Y. F.; Wachsman, E. D.; Hu, L. B., Transition from Superlithiophobicity to Superlithiophilicity of Garnet Solid-State Electrolyte. *J Am Chem Soc* **2016,** *138* (37), 12258-12262.
18. Ellis, B. L.; Lee, K. T.; Nazar, L. F., Positive Electrode Materials for Li-Ion and Li-Batteries†. *Chemistry of Materials* **2010,** *22* (3), 691-714.
19. Sakuda, A.; Hayashi, A.; Tatsumisago, M., Interfacial Observation between LiCoO2 Electrode and Li2S-P2S5 Solid Electrolytes of All-Solid-State Lithium Secondary Batteries Using Transmission Electron Microscopy. *Chemistry of Materials* **2010,** *22* (3), 949-956.
20. Haruyama, J.; Sodeyama, K.; Han, L. Y.; Takada, K.; Tateyama, Y., Space-Charge Layer Effect at Interface between Oxide Cathode and Sulfide Electrolyte in All-Solid-State Lithium-Ion Battery. *Chemistry of Materials* **2014,** *26* (14), 4248-4255.
21. Braun, S.; Yada, C.; Latz, A., Thermodynamically Consistent Model for Space-Charge-Layer Formation in a Solid Electrolyte. *J Phys Chem C* **2015,** *119*, 22281-22288.
22. Tsai, C. L.; Dashjav, E.; Hammer, E. M.; Finsterbusch, M.; Tietz, F.; Uhlenbruck, S.; Buchkremer, H. P., High Conductivity of Mixed Phase Al-Substituted Li7La3Zr2O12. *Journal of Electroceramics* **2015,** *35* (1-4), 25-32.
23. Murugan, R.; Thangadurai, V.; Weppner, W., Lattice Parameter and Sintering Temperature Dependence of Bulk and Grain-Boundary Conduction of Garnet-like Solid Li-Electrolytes. *Journal of The Electrochemical Society* **2008,** *155* (1), A90.
24. Murugan, R.; Thangadurai, V.; Weppner, W., Fast Lithium Ion Conduction in Garnet-Type Li7La3Zr2O12. *Angewandte Chemie International Edition* **2007,** *46* (41), 7778-7781.
25. Miara, L.; Windmuller, A.; Tsai, C. L.; Richards, W. D.; Ma, Q. L.; Uhlenbruck, S.; Guillon, O.; Ceder, G., About the Compatibility between High Voltage Spinel Cathode Materials and Solid Oxide Electrolytes as a Function of Temperature. *Acs Appl Mater Inter* **2016,** *8* (40), 26842-26850.

26. Fu, K.; Gong, Y.; Hitz, G. T.; McOwen, D. W.; Li, Y.; Xu, S.; Wen, Y.; Zhang, L.; Wang, C.; Pastel, G.; Dai, J.; Liu, B.; Xie, H.; Yao, Y.; Wachsman, E. D.; Hu, L., Three-Dimensional Bilayer Garnet Solid Electrolyte Based High Energy Density Lithium Metal–Sulfur Batteries. *Energy & Environmental Science* **2017,** *10* (7), 1568-1575.
27. Ohta, S.; Seki, J.; Yagi, Y.; Kihira, Y.; Tani, T.; Asaoka, T., Co-Sinterable Lithium Garnet-Type Oxide Electrolyte with Cathode for All-Solid-State Lithium Ion Battery. *Journal of Power Sources* **2014,** *265*, 40-44.
28. Liu, T.; Ren, Y. Y.; Shen, Y.; Zhao, S. X.; Lin, Y. H.; Nan, C. W., Achieving High Capacity in Bulk-Type Solid-State Lithium Ion Battery Based on Li6.75La3Zr1.75Ta0.25O12 Electrolyte: Interfacial Resistance. *Journal of Power Sources* **2016,** *324*, 349-357.
29. Becker-Steinberger, K.; Funken, S.; Landstorfer, M.; Urban, K., A Mathematical Model for All Solid-State Lithium-Ion Batteries. *ECS Transactions* **2010,** *25* (36), 285-296.
30. Bazant, M. Z.; Kilic, M. S.; Storey, B. D.; Ajdari, A., Towards an Understanding of Induced-Charge Electrokinetics at Large Applied Voltages in Concentrated Solutions. *Advances in Colloid and Interface Science* **2009,** *152*, 48-88.
31. Landstorfer, M.; Funken, S.; Jacob, T., An Advanced Model Framework for Solid Electrolyte Intercalation Batteries. *Physical chemistry chemical physics : PCCP* **2011,** *13*, 12817-25.
32. Danilov, D.; Niessen, R. A. H.; Notten, P. H. L., Modeling All-Solid-State Li-Ion Batteries. *Journal of The Electrochemical Society* **2011,** *158*, A215.
33. Fabre, S. D.; Guy-Bouyssou, D.; Bouillon, P.; Le Cras, F.; Delacourt, C., Charge⁄Discharge Simulation of an All-Solid-State Thin-Film Battery Using a One-Dimensional Model. *Journal of The Electrochemical Society* **2012,** *159*, A104.
34. Talin, A. A.; Ruzmetov, D.; Kolmakov, A.; McKelvey, K.; Ware, N.; El Gabaly, F.; Dunn, B.; White, H. S., Fabrication, Testing, and Simulation of All-Solid-State Three-Dimensional Li-Ion Batteries. *Acs Appl Mater Inter* **2016,** *8* (47), 32385-32391.
35. Doyle, M.; Fuller, T. F.; Newman, J., Modeling of Galvanostatic Charge and Discharge of the Lithium Polymer Insertion Cell. *Journal of the Electrochemical Society* **1993,** *140*, 1526-1533.
36. De Vidst, P.; White, R. E., Governing Equations for Transport in Porous Electrodes. *Journal of The Electrochemical Society* **1997,** *144*, 1343-1353.
37. Ramadass, P.; Haran, B.; Gomadam, P. M.; White, R.; Popov, B. N., Development of First Principles Capacity Fade Model for Li-Ion Cells. *Journal of The Electrochemical Society* **2004,** *151*, A196.
38. Latz, A.; Zausch, J., Thermodynamic Consistent Transport Theory of Li-Ion Batteries. *Journal of Power Sources* **2011,** *196*, 3296-3302.
39. Latz, A.; Zausch, J., Multiscale Modeling of Lithium Ion Batteries: Thermal Aspects. *Beilstein Journal of Nanotechnology* **2015,** *6*, 987-1007.
40. Garcia, R. E.; Chiang, Y. M.; Carter, W. C.; Limthongkul, P.; Bishop, C. M., Microstructural Modeling and Design of Rechargeable Lithium-Ion Batteries. *Journal of the Electrochemical Society* **2005,** *152* (1), A255-A263.
41. Goldin, G. M.; Colclasure, A. M.; Wiedemann, A. H.; Kee, R. J., Three-Dimensional Particle-Resolved Models of Li-ion Batteries to Assist the Evaluation of Empirical Parameters in One-Dimensional Models. *Electrochimica Acta* **2012,** *64*, 118-129.

42. Uhlenbruck, S.; Dornseiffer, J.; Lobe, S.; Dellen, C.; Tsai, C.-L.; Gotzen, B.; Sebold, D.; Finsterbusch, M.; Guillon, O., Cathode-Electrolyte Material Interactions During Manufacturing of Inorganic Solid-State Lithium Batteries. *Journal of Electroceramics* **2016**, 1-10.
43. Math2Market, GeoDict. *http://www.geodict.com* **2017**.
44. Latz, A.; Zausch, J., BEST - Battery and Electrochemistry Simulation Tool. *http://www.itwm.fraunhofer.de/best*.
45. Buschmann, H.; Dolle, J.; Berendts, S.; Kuhn, A.; Bottke, P.; Wilkening, M.; Heitjans, P.; Senyshyn, A.; Ehrenberg, H.; Lotnyk, A.; Duppel, V.; Kienle, L.; Janek, J., Structure and Dynamics of the Fast Lithium Ion Conductor "Li7La3Zr2O12". *Physical chemistry chemical physics : PCCP* **2011,** *13* (43), 19378-92.
46. Janani, N.; Deviannapoorani, C.; Dhivya, L.; Murugan, R., Influence of Sintering Additives on Densification and Li+ Conductivity of Al Doped Li7La3Zr2O12 Lithium Garnet. *RSC Adv.* **2014,** *4*, 51228-51238.
47. Molenda, J.; Stoklosa, A.; Bak, T., Modification in the Electronic-Structure of Cobalt Bronze LixCoO2 and the Resulting Electrochemical Properties. *Solid State Ionics* **1989,** *36* (1-2), 53-58.
48. Meibuhr, S. G., Electrode Studies in Nonaqueous Electrolytes. *Journal of The Electrochemical Society* **1970,** *118*, 1320.
49. Ren, Y.; Liu, T.; Shen, Y.; Lin, Y.; Nan, C.-W., Chemical Compatibility Between Garnet-Like Solid State Electrolyte Li6.75La3Zr1.75Ta0.25O12 and Major Commercial Lithium Battery Cathode Materials. *Journal of Materiomics* **2016,** *2* (3), 256-264.
50. Kato, Y.; Hori, S.; Saito, T.; Suzuki, K.; Hirayama, M.; Mitsui, A.; Yonemura, M.; Iba, H.; Kanno, R., High-Power All-Solid-State Batteries Using Sulfide Superionic Conductors. *Nat Energy* **2016,** *1*, 16030.
51. Yu, C.; Ganapathy, S.; Van Eck, E. R. H.; Wang, H.; Basak, S.; Li, Z. L.; Wagemaker, M., Accessing the Bottleneck in All-Solid State Batteries, Lithium-Ion Transport Over the Solid-Electrolyte-Electrode Interface. *Nat Commun* **2017,** *8*, 1086.
52. Sakuda, A.; Kitaura, H.; Hayashi, A.; Tadanaga, K.; Tatsumisago, M., All-Solid-State Lithium Secondary Batteries with Oxide-Coated LiCoO2 Electrode and Li2S-P2S5 Electrolyte. *Journal of Power Sources* **2009,** *189* (1), 527-530.
53. Ohta, S.; Kobayashi, T.; Seki, J.; Asaoka, T., Electrochemical performance of an all-solid-state lithium ion battery with garnet-type oxide electrolyte. *Journal of Power Sources* **2012,** *202*, 332-335.
54. Gallaghera, K. G.; Traska, S. E.; Bauer, C.; Woehrle, T.; Lux, S. F.; Tschech, M.; Lamp, P.; Polzin, B. J.; Ha, S.; Long, B.; Wu, Q.; Lu, W.; Dees, D. W.; Jansena, A. N., Optimizing Areal Capacities through Understanding the Limitations of Lithium-Ion Electrodes. *J. Electrochem. Soc.* **2016,** *163* (2), A138-A149.

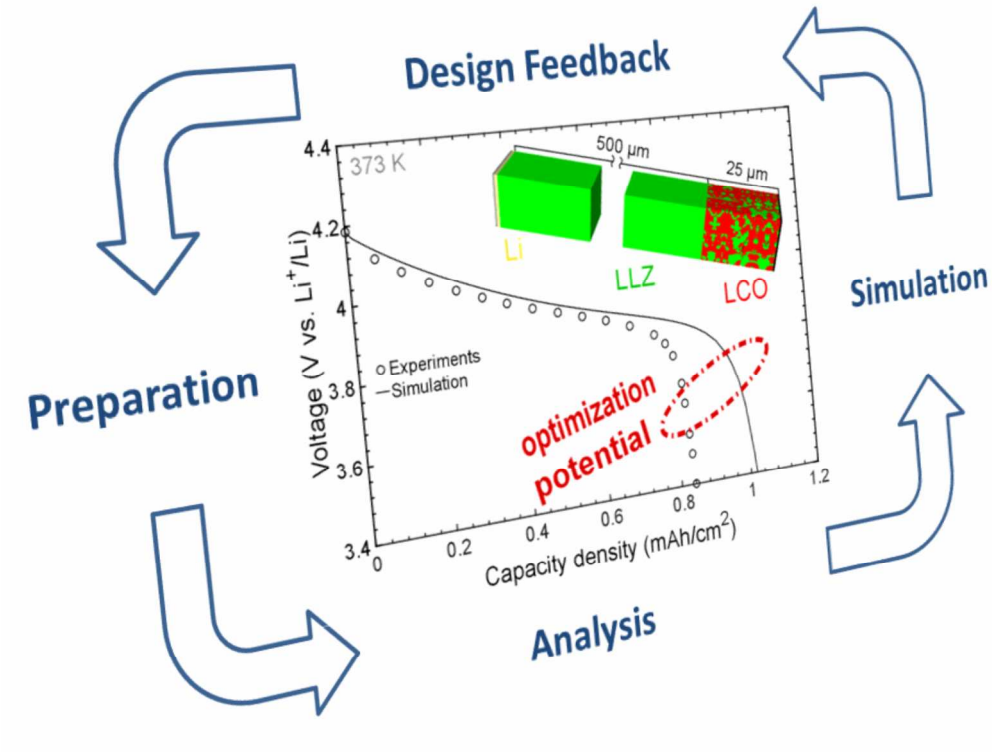

TOC graphic

242x182mm (300 x 300 DPI)